Journal of the Korean Nuclear Society
Volume 18, Number 1, March 1986

Radiation Streaming in KNU-1 Reactor Cavity

Kun-Woo Cho and Chang-Soon Kang
Seoul National University
(Received January 10, 1986)

고리 1호기 원자로 공동에서의 방사선 흐름 현상 해석

조 건 우·강 창 순
서울대학교
(1986. 1. 10 접수)

Abstract

The neutron fluxes and dose rates due to radiation streaming from reactor cavities were evaluated at the KNU-1 reactor pressure vessel (RPV) head flange elevation. To find a suitable cross section data set for the evaluation, a benchmark test was performed for three data sets; DLC-23/CASK, DLC-31/FEWG, and DLC-47/BUGLE. The leakage fluxes from the KNU-1 RPV outer surface were calculated with two different methods; 1-D calculation with ANISN, and 2-D calculation with DOT3.5. The Monte Carlo procedures as embodied in the MORSE-CG code combined with the albedo option were applied to predict the radiation distributions in the cavity region. Finally, the activation analysis of the stud bolts was performed to identify the major activation products.

요 약

본 논문에서는 고리 1호기의 원자로 압력용기와 1차 콘크리트 차폐체 사이의 원자로 공동에서의 방사선 흐름 현상을 평가하였다. 원자로 압력용기 외부 표면에서 방출되는 누출 선속을 계산하기 위해 사용될 적합한 중성자 단면적 자료를 얻기 위하여, DLC-23/CASK, DLC-31/FEWG 그리고 DLC-47/BUGLE 등 세가지의 중성자 단면적 자료에 대한 검증 계산을 수행하였다. 누출 선속 계산은 ANISN으로 1차원적 계산을, DOT3.5로 2차원적 계산을 수행하였으며, 또한 원자로 공동에서의 방사선 흐름 현상을 분석하기 위하여, 알베도 개념이 도입된 몬테카를로 방법을 사용하는 MORSE-CG 전산 코드를 이용하여 3차원적 해석을 하였다. 그리고, 원자로 플랜지 부위에서의 방사화 분석을 수행하여 스터드 볼트의 방사화 정도를 평가하였다.

I. Introduction

Experiences at operating PWR's have revealed that the air cavities between the reactor pressure vessel(RPV) and the primary shield wall can provide paths for radiation streaming, which may prohibitively limit the accessibility required to certain areas in the containment during power operation, and cause an undesirable radiation environment to the equipment and the cables located above the vessel. The radiation streaming in the cavity of a PWR occurs in two steps: transport of source neutrons from the core to the outer surface of the RPV through dense reactor materials, and transport in the near cavity including the interaction of the neutrons with the steel and concrete which comprise the

boundary of the cavity region. In this paper, the dose rate is evaluated at the RPV flange level of KNU-1 due to radiation streaming through the annular reactor cavity. This paper is divided into four basic sections:

1) Benchmark test of cross section data sets which will be used in the source term and streaming calculations.
2) Source term calculation which is the calculation of leakage flux from the RPV outer surface.
3) Streaming calculation which is the evaluation of dose rate at the RPV flange level due to radiation streaming through the annular reactor cavity.
4) Neutron activation analysis of the RPV head stud bolts.

For the benchmark test of cross section data sets, a 1-D discrete ordinates transport code ANISN[1] was employed. And ANISN, and a 2-D discrete ordinates transport code DOT3.5[2] were employed with the DLC-23/CASK[3] cross section data set which was found to be most appropriate through the benchmark test for source term calculations, in which we computed the neutron anguar flux leaking from the RPV outer surface. For the analysis of neutron streaming through reactor cavities, a Monte Carlo technique of which an albedo collision model is coupled to the normal random walk was used. The MORSE-CG[4] computer code package along with the modified BREESE[5] module for implementing the albedo option was employed with the 22-group neutron cross section data set (DLC-23/CASK) and 17-group neutron albedo data set for concrete.[6,7,8,9] The neutron activation analysis of stud bolts was conducted using the DLC-51/JSD-120[10] activation cross section data set which was collapsed from 100 group structure to DLC-23/CASK 22 group structure using the weighting spectrum generated by ANISN.

II. Benchmark Test of Cross Section Data Set

The purpose of the benchmark test is to select the best suitable cross section data set for an input to the source term calculation. ANS 6.2 benchmark problem No. 2,[11] which has a very similar geometry to this source term calculation, was analyzed with three data sets; DLC-23/CASK, DLC-31/FEWG,[12] and DLC-47/BUGLE.[13] The ANISN calculation was perfo-rmed with an S_8 angular quadratures, a P_3 Legendre expansion of the scattering matrices and a convergence criterion of 1×10^{-4}. Neutron dose rates were calculated using the flux-to-dose rate conversion factors given in an analytic function:[14]

$$\ln DF(E) : A+BX+CX^2+DX^3$$

where

$DF(E)$: flux-to-dose rate factor at energy E (rem/hr)/(n/cm^2-sec)

E : neutron energy in MeV

X : ln E (natural logarithm)

A, B, C, D : the coefficients given in Ref. 14.

The resulting neutron dose rates at various locations are given in Table 1. It shows that

Table 1. Neutron Dose Rate (rem/hr)/(neutron/cm-sec) Calculated with Different Cross Section Sets at the Specific Locations

Locaions \ Data set	DLC-47 BUGLE	DLC-31 FEWG	DLC-23 CASK
In Core	1.34-08*	+ 4.3%	+ 2.6%
Barrel inside	1.10-09	+ 9.9%	+ 5.7%
Coolant inside	7.46-10	+ 8.7%	+ 3.6%
In Coolant	2.38-10	+ 8.6%	+ 6.5%
Baffle inside	7.91-11	+10.6%	+ 9.1%
Coolant inside	3.47-11	+ 8.6%	+ 6.5%
In Coolant	2.82-11	+ 8.6%	+ 7.1%
RPV inside	1.56-12	+ 9.9%	+12.9%
In RPV	9.27-13	+11.6%	+12.0%
Air gap inside	2.66-13	+ 4.9%	+ 3.8%
Concrete inside	2.47-13	+ 5.3%	+4.5%

* Read as 1.34×10^{-8}

the calculation with the DLC-23/CASK library slightly overestimates the dose rates by 3~13% depending on the locations compared to the DLC-47/BUGLE calculation and agrees well within 4% with the DLC-31/FEWG calculation. Hence, it is concluded that DLC-23/CASK is conservative and good enough to be used for this work.

III. Source Term Calculations

To evaluate the neutron cavity streaming, it is essential to know the neutron angular fluxes which escape the RPV outer surface. The leakage fluxes were calculated by two different methods;

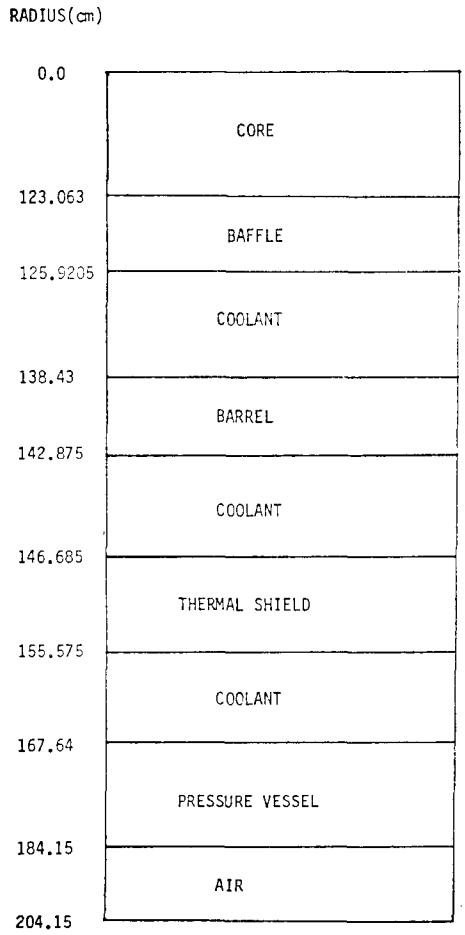

Fig. 1. Radial One-Dimensional Configuration of KNU-1 (not to scale)

Table 2. Material Specifications of KNU-1 Reactor

REGION	MATERIAL
Core	LWR Homogeneous core
Baffle	Stainless Steel
Coolant	Borated Primary Coolant
Barrel	Stainless Steel
Coolant	Borated Primary Coolant
Thermal Shield	Stainless Steel
Coolant	Borated Primary Coolant
Pressure Vessel	Low Carbon Steel
Air Gap	Air

1-D calculation with ANISN, and 2-D calculation with DOT3.5. The results of these two independent calculations were compared and used in the subsequent MORSE-CG Monte Carlo analysis of radiation streaming through the reactor cavity. Fig 1 describes the model of KNU-1 reactor used in the calculations. Material specification are given in Table 2 and the atom densities used for mixing are given in Table 3. To obtain the detailed power distribution, which is one of the important factors to determine the neutron leakage flux, in the core of KNU-1 at the beginning of life, a few group diffusion code based on finite difference method, KIDD,[15] was used. The radial power distribution of KNU-1 is given in Table 4 which was converted from two-dimensional KIDD output to equivalent one-dimensional distribution.

3.1. ANISN Calculation

The energy and angular distribution of the neutrons leaving the RPV at the core midplane was calculated by ANISN. The calculation were performed with a completely symmetric S_{12} quadrature set containing 48 discrete angles in the cylindrical geometry, a P_3 Legendre expansion of the scattering matrices and a convergence criterion of 1.0×10^{-4}. The total number of mesh point was 172 of which the intervals were small enough so that the flux did not vary by more than a factor of two between adjacent mesh

Table 3. Mixing Table for Source Term Calculation. (atoms/barn-cm)

	Core	Water	SS-304	Carbon Steel	Air	Concrete
H	3.726-02	5.02-02	—	—	—	7.77-03
B-10	6.514-06	6.937-06	—	—	—	—
C	1.831-06	—	—	8.67-04	—	—
N	—	—	—	—	4.25-05	—
O	3.304-02	2.51-02	—	—	1.13-05	4.39-02
Na	—	—	—	—	—	1.05-03
Mg	—	—	—	—	—	1.49-04
Al	2.551-06	—	—	—	—	2.39-03
Si	6.60-06	—	—	4.96-04	—	1.58-02
K	—	—	—	—	—	6.93-04
Ca	—	—	—	—	—	2.92-03
Ti	2.586-06	—	—	—	—	—
Cr	1.077-04	—	1.74-02	1.54-04	—	—
Mn	5.871-06	—	1.52-03	1.12-03	—	—
Fe	2.176-04	—	5.81-02	8.20-02	—	3.13-04
Ni	1.447-04	—	8.51-03	5.95-04	—	—
Zr	4.104-03	—	—	—	—	—
Mo	7.235-06	—	—	2.71-04	—	—
Sn	4.818-05	—	—	—	—	—
U-235	1.941-04	—	—	—	—	—
U-238	6.893-03	—	—	—	—	—

Table 4. Radial Power Distribution of KNU-1 (BOL)

RADIUS (cm)	RELATIVE POWER	RADIUS (cm)	RELATIVE POWER
0.0	1.043	81.0	1.083
9.0	1.035	90.0	1.066
18.0	1.032	99.0	1.004
27.0	1.041	108.0	0.863
36.0	1.051	116.8	0.632
45.0	1.034	121.1	0.537
54.0	1.059	122.4	0.494
63.0	1.051	122.96	0.493
72.0	1.099	123.063	0.445

points.[16] The source of neutrons was derived from the mean power density by assuming 7.62×10^{10} neutrons emitted per watt. The shape of the radial distribution of fission densities within the core is taken as the relative power rating of fuel assemblies as shown in Table 4.

3.2. DOT3.5 Calculation

The RPV leakage flux which is the function of space, energy, and angle was calculated in a two dimensional cylindrical $R-Z$ geometry using the DOT3.5 computer code with P_3-S_8 approximation. The vacuum boundary condition external to the pressure vessel was employed. The geometry of KNU-1 core and RPV was described by 26 radial and 26 axial intervals. The SORREL[17] computer code generated the input tape of 2-D volumetric source from the two dimensional KIDD output. A single run of DOT3.5 provides the total scalar flux tape by group and spatial interval, the angular flux tape by group, spatial interval, and the angle, and boundary angular flux tape at a radial and/or axial boundary of the system, which are used for the subsequent analysis of cavity streaming.

3.3. Results of the Source Term Calculations

The results of the ANISN calculation are presented in Tables 5 and 6, and in Figures 2 and 3. Tables 5 and 6 show the neutron leakage fluxes from the RPV outer surface at the mid-

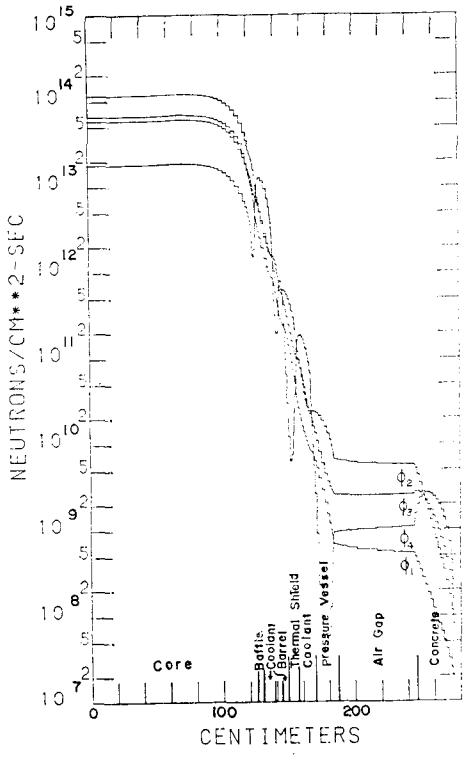

Fig. 2. Radial Variations of Four Group Neutron Fluxes on the Core Mid-Plane

plane of the core. Figure 2 shows the radial variations of neutron fluxes through the reactor internals and the pressure vessel. In Figure 2 and Table 6, the nutreon fluxes are collapsed and presented in four energy groups: 15.0∼1.11 MeV, $1.11-3.35\times10^{-3}$MeV, $3.35\times10^{-3}-4.14\times10^{-7}$MeV and thermal energy. Fig 3 illustrates the energy spectra at the various locations on the core mid-plane. In the RPV, the neutron energy spectrum changes substantially since the iron inelastic scattering very quickly attenuates the high-energy neutrons relative to those at lower energies. In the KeV energy range, the neutron transmission is quite high due to the minima in the iron cross section, which shows up quite prominently around 25 KeV.[18] The axial variation in the fluence at the RPV outer surfaces calculated by DOT3.5 depends on the equilibrium cycle burnup profile in the core, and

Table 5. Neutron Fluxes at the Outer Surface of the Reactor Pressure Vessel(at the Mid-Plane)

Group	Upper Energy*(eV)	Flux(n/cm²-sec)
1	1.492+07	1.201+06
2	1.22 +07	4.580+06
3	1.00 +07	1.088+07
4	8.18 +06	2.256+07
5	6.36 +06	3.942+07
6	4.96 +06	3.437+07
7	4.06 +06	6.223+07
8	3.01 +06	8.140+07
9	2.46 +06	2.764+07
10	2.35 +06	1.658+08
11	1.83 +06	6.058+08
12	1.11 +06	1.870+09
13	5.50 +05	4.925+09
14	1.11 +05	3.395+09
15	3.35 +03	9.913+08
16	5.83 +02	8.552+08
17	1.01 +02	6.003+08
18	2.90 +01	3.965+08
19	1.01 +01	4.360+08
20	3.06 +00	3.043+08
21	1.12 +00	2.474+08
22**	4.14 −01	1.200+09

* DLC-23/CASK 22 group structure
** lower energy; 1.0-2

Table 6. Radial Four-Group Neutron Leakages outside Reactor Vessel on the Core Mid-Plane

Energy Group	Energy Interval	Neutron Flux (n/cm²-sec)
1	1.11Mev$<E$	1.056+09
2	3.35Kev$<E\leq$1.11 Mev	1.019+10
3	0.414eV$<E\leq$3.35 Kev	3.831+09
4	0.01eV$<E\leq$0.414 eV	1.200+09

the flux is rapidly falling off above and below the core mid-plane area. The axial peak-to-mean factor is 1.44. Table 7 shows the ANISN one-dimensional fluxes and with the DOT3.5 two-dimensional fluxes near the surface of the RPV on the core mid-plane. The results of ANISN slightly overestimates in all energy bins except for the thermal energy bin compared to those of

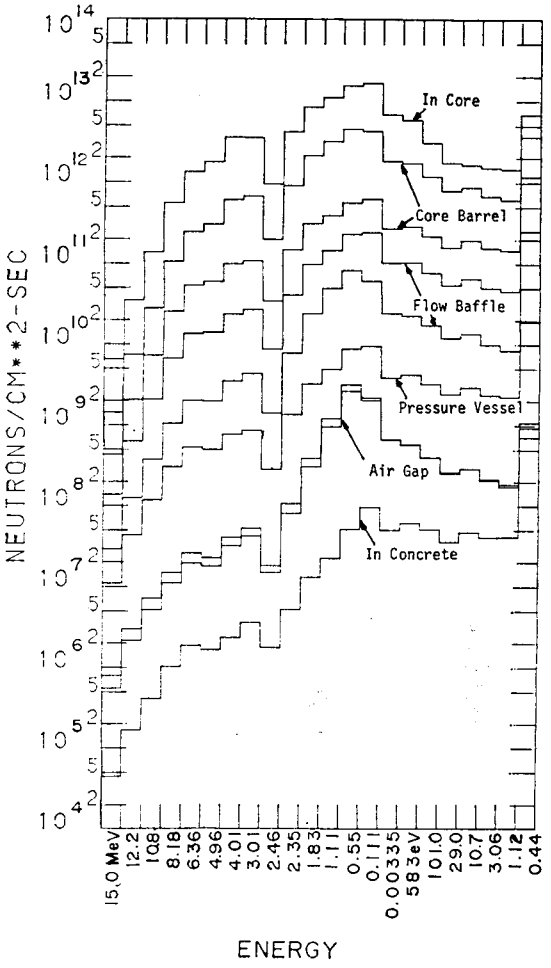

Fig. 3. Neutron Spectra for KNU-1 at various radial positions on the Core Mid-Plane

DOT3.5, which is expected since the particle transports in the axial direction are neglected in ANISN.

IV. Streaming Calculation

Several techniques and combinations of techniques have been used to perform the analysis of radiation streaming in reactor cavities.[18),19),20)] They include the discrete ordinates transport models (Sn procedures), multidimensional Monte Carlo techniques, combined albedo and Monte Carlo procedures, and simple "hand-book" hand calculational method. In this work, the Monte

Table 7. DOT 3.5 and ANISN Neutron Fluxes (n/cm²-sec) at the Core Mid-Plane

Group	DOT 3.5(r=181.7cm)	ANISN(r=181.45cm)
1	1.746+06	1.838+06
2	6.678+06	7.017+06
3	1.504+07	1.699+07
4	2.825+07	3.622+07
5	4.893+07	6.372+07
6	3.829+07	5.537+07
7	7.871+07	1.017+08
8	1.021+08	1.335+08
9	3.532+07	4.541+07
10	2.423+08	2.852+08
11	8.407+08	9.917+08
12	2.344+09	2.861+09
13	5.781+09	7.684+09
14	3.412+09	5.607+09
15	5.678+08	1.258+09
16	5.083+08	1.005+09
17	4.185+08	7.492+08
18	3.649+08	5.376+08
19	3.649+08	5.383+08
20	2.806+08	3.118+08
21	2.220+08	1.912+08
22	6.546+08	1.841+08

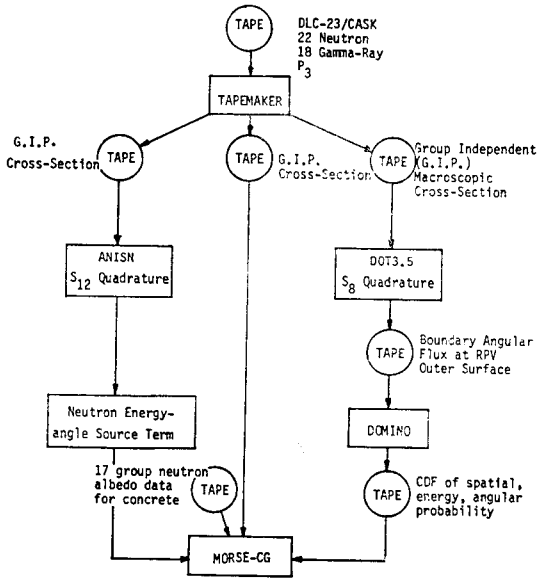

Fig. 4. Sequence of Calculation Used to Obtain the Neutron Energy Spectra at RPV Flange Level.

Carlo procedure as embodied in the MORSE-CG code combined with albedo was applied to predict the radiation distributions in the cavity region.

The sequence of radiation transport calculations used to obtain the neutron energy spectra and dose rates at the RPV head flange elevation in KNU-1 reactor cavity is shown in Figure 4. The calculational sequence incorporates both discrete ordinates and Monte Carlo radiation transport method.

4.1. Source

This calculation is accomplished by initiating neutron histories at the annular cylindrical shell along the outer surface of the RPV. The 2-D RPV leakage fluxes calculated by DOT3.5 were input to the DOMINO[21] computer code which generated the source for the subsequent 3-D Monte Carlo analyses of the radiation streaming in the reactor cavity and thence to the points of interest within the containment building. DOMINO provides the cumulative distribution functions in energy, space, and in polar and azimuthal angular fluence as subsequent source input to MORSE-CG.

4.2. Geometry

One of the pheripheral problems which we have encountered, relates to the complicated geometries and its representation in the calculational model. Even though a particular geometry may be quite simple, MORSE-CG, because of the prediction and tolerance used in tracking, may not still be able to completely follow the particle. In this case, the well-described gometry to remove possible ambiguities will sometimes remove these tracking errors. The adequacy and accuracy of the geometrical model was checked by comparing the design drawings with the computer generated pictures representing selected sections of the model by the computer code, PICTURE-CG.[22]

4.3. Albedo Option in MORSE-CG with Modified BREESE

For many reactor radiation streaming problems, the interactions of neutrons in the boundaries of the cavity may be represented by the loss of the particles in the boundaries and their re-emission into the cavity. An Actual analysis of these interactions by Monte Carlo requires a very long computation time. Therefore, the simplified analysis of considering the wall interaction by using the albedo concept is a useful and practical way to improve calculational efficiency. The doubly differential angular albedos were incorporated into the MORSE-CG Monte Carlo code. The concrete albedo data for 17 neutron groups, 5 incident angles, and 30 reflected angles, which is based on the data generated by Maerker and Muckenthaler et al., was used in the calculations.

The BREESE albedo routine attached to the MORSE-CG code handles the albedo data specified by the energy and the polar and azimuthal angles of scattered neutrons. The energy, direction, and weight of scattered neutrons at an albedo surface are calculated using the albedo data and the weight of incident neutrons.

In using the albedo option in MORSE-CG, user-written subroutines ALBIN, ALBDO, and THETO must be included. The subroutine NESXE(N) employs a statistical estimation procedure to calculate the next-flight contribution to the detector from an albedo collision. NESXE (N) is also called from BANKR(6). Meanwhile, in case of a combination problem of transport and albedo, there should be a correspondence between the finer group cross-section data structure and the broader group albedo structure. There is little difficulty in composing broad group from fine group. The reverse correspondence requires an assumption that the energy spectral shape within a broad group as can be decomposed into fine groups within the broad group in the same way as the cross sections in the fine group structure were weighted, i.e., 1/E.[23]

4.4. Other Inputs and Importance Sampling

A SOURCE subroutine was written for the area source at the RPV outer surface. Neutron histories were started just at the exterior surface of the RPV in order to clarify the zone specification of source position. A good definition of the angular distribution of the fast-neutron leakage from the pressure vessel is a prerequisite for an accurate analysis. Especially in case of calculating with ANISN source, the source particle parameters were selected in such a way that the locations from a flat azimuthal spatial distribution, directions from an isotropic polar angle distribution and from the supplied azimuthal angles distribution, and energies from the supplied energy groups.

Considerable efforts have been undertaken to increase the efficiency of the MORSE-CG analyses, by using appropriate important sampling techniques as well as the coupled Monte Carlo-albedo scattering treatment. These techniques included source energy biasing, source position biasing, source direction biasing, Russian Roulette and splitting, and use of different exponential transformation parameters as a function of region and energy. A flat source energy distribution was used and the source particle positions were selected with appropriate weight correction with the following biasing probability:

$$P(Z)=3/4,\ Z>0$$
$$=1/4,\ Z\leqslant 0$$

The polar angle of source direction was selected from between 0° and 90° which can contribute to the detector at the RPV flange elevation, but for the justification of this biasing, the initial

Table 8. Neutron Flux at Flange Elevation(n/cm²-sec) (Calculated with ANISN Source as a Function of Cavity Width)

Group \ Gap size	80cm	70cm	60cm
1	—	—	—
2	—	—	—
3	—	—	—
4	—	—	—
5	—	—	—
6	6.15+03(.206)*	3.97+03(.301)	2.96+03(.446)
7	1.82+04(.266)	1.34+04(.275)	1.59+04(.276)
8	1.50+04(.404)	8.79+03(.476)	1.47+04(.424)
9	2.99+03(.244)	3.00+03(.320)	1.02+03(.562)
10	1.06+05(.191)	8.17+04(.227)	1.44+05(.301)
11	5.71+05(.370)	4.69+05(.480)	3.37+05(.680)
12	1.41+07(.246)	1.25+07(.329)	1.38+07(.288)
13	6.58+07(.253)	6.92+07(.328)	5.19+07(.378)
14	1.03+08(.178)	8.91+07(.199)	1.15+08(.367)
15	2.07+07(.214)	2.15+07(.545)	2.29+07(.336)
16	8.56+06(.390)	7.90+06(.315)	5.87+06(.425)
17	3.80+06(.200)	3.64+06(.308)	5.55+06(.291)
18	1.18+06(.245)	2.85+06(.367)	3.35+06(.607)
19	6.05+05(.245)	5.62+05(.334)	1.55+05(.631)
20	2.68+06(.315)	1.04+06(.279)	9.18+05(.259)
21	2.04+06(.236)	2.09+06(.231)	4.38+05(.318)
22	3.21+07(.135)	2.80+07(.161)	2.58+07(.168)
Total	2.56+08(.112)	2.39+08(.135)	2.46+08(.193)

*; fractional standard deviation

Table 9. Neutron Flux at Flange Elevation(n/cm²-sec) (Calculated with DOT 3.5 Source as a function of Cavity Width)

Group \ Gap size	80cm	70cm	60cm
1	—	—	—
2	—	—	—
3	—	—	—
4	—	—	—
5	—	—	—
6	1.52+03(.386)*	2.98+03(.378)	1.62+03(.556)
7	1.14+04(.361)	4.78+03(.492)	1.21+04(.430)
8	3.46+04(.371)	1.76+04(.359)	3.88+04(.513)
9	1.72+03(.526)	3.61+03(.564)	3.88+04(.513)
10	3.82+04(.513)	1.31+05(.396)	8.06+04(.544)
11	3.08+06(.617)	6.82+05(.718)	6.56+05(.876)
12	4.49+06(.569)	1.01+07(.356)	4.39+06(.669)
13	1.57+08(.273)	5.92+07(.452)	7.04+07(.411)
14	9.01+07(.240)	9.10+07(.186)	8.26+07(.291)
15	7.34+06(.298)	3.40+06(.278)	1.07+07(.390)
16	2.69+06(.387)	2.42+06(.488)	3.94+05(.314)
17	1.55+06(.334)	1.50+06(.372)	2.08+06(.369)
18	1.31+06(.236)	1.84+06(.350)	1.08+06(.390)
19	1.22+05(.478)	1.58+05(.361)	4.67+04(.977)
20	1.99+06(.342)	7.52+05(.292)	2.19+06(.427)
21	2.63+06(.618)	5.62+05(.226)	1.24+06(.793)
22	9.99+06(.135)	1.08+07(.150)	1.02+07(.267)
Total	2.83+08(.173)	1.82+08(.200)	1.86+08(.198)

*; fractional standard deviation

starting weight of each history should be taken as 0.5. The exponential transform with the PATH of 0.5 in combination with the DIREC function which stretches path length toward $+Z$ direction.

The scoring was done by next-event surface crossing estimation of the flux to the areas of interest, and only energy distributions are calculated. The pseudo-disk-detector is located at the RPV head flange elevation, and this disk was divided into a number of concentric rings with equal 10cm intervals. For the uncollided flux and dose at the RPV flange gap, the estimation was performed at BANKR(1) via the NESXE(N) subroutine, and the contribution of scattered neutrons from each collision point and reflecting point at albedo medium were performed at BANKR(5) and BANKR(6), respectively.

4.5. Results

The results of streaming calculation with MORSE-CG are presented in Tables 8 and 9. They were computed with the two different sources calculated using ANISN and DOT 3.5. As the gap size of reactor cavity varies from 60 to 80 centimeters, the resulting neutron fluxes and dose rates increase nearly linearly. And, neutrons with energies greater than 1.83MeV (groups 1 to 10) in the reactor cavity annular region do not contribute significantly to the dose rates at the pressure vessel head flange elevation.

V. Activation Calculation

The neutron activation of RPV head stud

Table 10. Acvity vs. Time after Shutdown (units; dps per unit volume)

Radioisotopes \ Time after* Shutdown	0HR	1DAY	3DAY	1MONTH	2MONTH
$Fe^{54}(n,\gamma)Fe^{55}$	8.56+04	8.55+04	8.54+04	8.37+04	8.19+04
$Mo^{98}(n,\gamma)Mo^{99}$	3.85+03	3.40+03	1.82+03	2.17+00	1.22−03
$Mo^{100}(n,\gamma)Mo^{101}$	1.14+03	1.62−12	0.0	0.0	0.0
$Fe^{54}(n,p)Mn^{54}$	2.30+01	2.30+01	2.29+01	2.15+01	2.01+01
$Ni^{58}(n,p)Co^{58}$	9.42+00	9.38+00	9.15+00	7.04+00	5.26+00

* Assumed that KNU-1 operates for 300 days at its nominal power

Thable 11. Acvity vs. Reactor Operating Year (units; dps per unit volume)

Radioisotopes \ Reactor* Operation Time	1YEAR	3YEAR	10YEAR	20YEAR	30YEAR
$Fe^{54}(n,\gamma)Fe^{55}$	8.19+04	1.93+05	3.26+05	3.48+05	3.50+05
$Mo^{98}(n,\gamma)Mo^{99}$	1.22−03	1.22−03	1.22−03	1.22−03	1.22−03
$Fe^{54}(n,p)Mn^{54}$	2.01+01	3.26+01	3.55+01	3.55+01	3.55+01
$Ni^{58}(n,p)Co^{58}$	5.26+00	5.41+00	5.41+00	5.41+00	5.41+00

* Assumed that KNU-1 operates for 300 days at its nominal power and cools down for 2 months after reactor shutdown.

bolts due to cavity streaming neutron was carried out using the DLC-51/JSD-120 activation cross section data set. The major activation processes were (n,γ), (n,p), (n,d), and $(n,2n)$ reactions.

To collapse the DLC-51/JSD-120 100 group structure to DLC-23/CASK 22 group structure, ANISN calculation was performed to generate the weighting spectrum. The results of activation calculation are presented in Tables 10 and 11. The dominant activation products are found to be Fe-55, Mo-99, Mn-54 and Co-58. All activation products except Fe-55 easily go to their equilibrium state within a few years of reactor operation time. The most important activation reaction in the stud-bolt irradiation was found to be Fe-54 (n,γ) Fe-55, where Fe-55 goes to its equilibrium in 10 years or so.

VI. Conclusions

An approach of studying radiation streaming effects due to a reactor cavity annulus as a function of gap distance is presented. In this approach, we found that the DLC-23/CASK cross section data set was good enough to perform the evaluation of the RPV leakage flux and the DOT-DOMINO-MORSE calculational sequence easily and properly treated the complex cavity streaming problems. Some modifications and improvements have been made to MORSE-CG to implement the albedo data base. Briefly, these are:

1) incorporation of the large data base without extensive use of computer core memory,

2) implementation of corresponding different energy group structures between albedo and cross-section data sets,

3) incorporation of a next-event surface crossing estimator which estimates uncollided contribution at each source position, and collided contribution at each real collision point and at each reflection position of the albedo medium.

References

1. W.W. Engle, Jr., "ANISN, A One Dimensional Discrete Ordinates Transport Code," K-1693, Oak Ridge Gaseous Plant, (1968).

2. W.A. Rhoades, "DOT3.5 Two Dimensional Discrete Ordinates Radiation Transport Code," Oak Ridge National Laboratory, RSIC CCC-276 (1975).
3. "CASK, 40 Group Coupled Neutron and Gamma-Ray Cross-Section Data," ORNL RSIC DLC-23 (1975).
4. M.B. Emmett, "The MORSE Monte Carlo Radiation Transport Code System," ORNL-4972 (1975).
5. V.R. Cain, "BREESE, Auxiliary Routines for Implementing the Albedo Option in the MORSE Code," G.P.D-Nuclear T.d. 4.
6. R.E. Maerker and F.J. Muckenthaler, "Calculation and Measurement of the Fast-Neutron Differential Dose Albedo for Concrete," Nucl. Sci. Eng., 22, 455-462 (1965).
7. R.E. Maerker and F.J. Muckenthaler, "Measurements and Single-Velocity Calculations of Differential Angular Thermal Neutron Albedos for Concrete," Nucl. Sci. Eng., 26, 399 (1966).
8. R.E. Maerker and F.J. Muckenthaler, "Monte Carlo Calculations Using the Albedo Concept of the Fast-Neutron Dose Rates along the Center Lines of One-and Two-Legged Square Concrete Open Ducts and Comparison with Experiment," Nucl. Sci. Eng., 27, 423-432 (1967).
9. J.T. Routti and M.H. Van De Voorde, "Estimates of Neutron Age Through Penetrations of the Cern Intersecting Storage Rings by Monte Carlo Albedo Calculations," Nucl. Eng. Des., 34, 293 (1975).
10. "Coupled 100 Neutron and 20 Gamma-Ray Effective Multigroup Cross Sections for Use in LWR and LMFBR Shield Design and Analysis," ORNL/RSIC DLC-51 (1978).
11. "Reactor Shielding Benchmark No. 2 for a PWR," NEACRP-L-151 (1976).
12. D.E. Bartine, et al., "DLC-31:37 Neutron, 21 Gamma-Ray Coupled, P3 Multigroup Library in ANISN Format," ORNL-RSIC DLC-31(1975).
13. "Coupled 45 Neutron, 16 Gamma-Ray, P3, Cross Sections for Studies by the ANS 6.1.2 Shielding Standards Working Group on Multigroup Cross Sections," ORNL/RSIC DLC-47 (1977).
14. American National Standard N666 (ANS-6.1), "Neutron and Gamma-Ray Flux-to-Dose Rate Factors" (1975).
15. S.K. Lee, K.S. Moon, B,J. Jun, and J.B. Lee, "KIDD, A KAERI-Improved Diffusion-Depletion Program for Nuclear Reactor Analysis," Korea Advanced Energy Research Institute (to be published)
16. R.G. Soltesz and R.K. Disney, WANL-PR-(LL)-034, Volume 4, "One-Dimensional Transport Technique," (1970).
17. J.T. West, "SORREL code Manual," Bsbcock & Wilcox Company (1975).
18. "Radiation Streaming in Power Reactors," ORNL/RSIC-43 (1979).
19. K. Ueki, "Three-Dimensional Neutron Streaming Calculations Using the Monte Carlo Coupling Technique," Nucl. Sci. Eng., 79, 253-264 (1981).
20. K. Shin, R. Murakami, H. Taniuchi, T. Hyodo, and Y. Oka, "Measurements of Neutron and Gamma-Ray Streaming in a Cavity-Duct System and an Analysis by an Albedo Monte Carlo Method," Nucl. Sci. Eng., 81, 161-171 (1982).
21. M.B. Emmett, C.E. Burgart and T.J. Hoffman, "DOMINO, A General Purpose Code for Coupling Discrete Ordinates and Monte Carlo Radiation Transport Calculations," ORNL-4853 (1973).
22. D.C. Irving and G.W. Morrison, "PICTURE: An Aid in Debugging GEOM Input Data," ORNL-TM-2892 (1970).
23. B.F. Maskewitz and V.Z. Jacobs, "A Review of the Monte Carlo Method for Radiation Transport Calculations," ORNL-RSIC-29 (1971).